Smart Rocks and Wireless Communication Systems for Real-Time Monitoring and Mitigation of Bridge Scour
(Progress Report No. 8)

Contract No: RITARS-11-H-MST
(Missouri University of Science and Technology)

Reporting Period: April 1 - June 30, 2013

PI: Genda Chen
Co-PIs: David Pommerenke and Y. Rosa Zheng

Program Manager: Mr. Caesar Singh

Submission Date: July 15, 2013

TABLE OF CONTENTS

EXECUTIVE SUMMARY

In the eighth quarter, more laboratory and field tests in a lake were conducted to understand the performance of new versions of both passive and active smart rocks. Emphasis was placed on the characterization of prototype passive rocks including a gravity-oriented design, new development of controllable magnet active smart rock, additional design and implementation of circuitry for magnet flipping, and development of active rock localization schemes using intensity in magneto-inductive communication and phase difference in acoustic communication.

For static magnetic field measurements, prototype passive rocks that were previously deployed and tested at bridge sites were used to develop a more accurate set of characteristics/calibration curves to relate the magnetic intensity to both measurement distance and magnet orientation. Furthermore, a gravity-oriented passive smart rock is being designed and tested to ensure that the magnet is always in alignment with the gravity field so that the effect of magnet orientation on the intensity-distance relation can be removed.

A new design of prototype active smart rocks with embedded magnets controlled by externally wrapped coils were fabricated and tested. The active rocks with controllabe magnets were made of an inner ball with one embedded magnet placed inside a sphere filled with high viscousity fluid between the ball and the sphere so that a “frictionless” interface can be created and the magnet can be flipped under current. Finally a coil was wrapped outside the sphere, with the designed circuitry, to flip the magnet as alternating current is supplied. The previously designed PCB board was modified and used to control magnets in the controllable magnet active rocks. In the following quarter, a new way of implementing controllable magnet active rocks with a gyroscope device will be designed and tested to further reduce the demand on the external power to flip magnet.

For active smart rocks with magneto-inductive communication, a new low frequency receiver was used to increase the sensitivity of the proposed localization scheme based on the change in strength. The new receiver unit electronic assembly with four boards housed in one compact box performs received Smart Rock signal filtering, amplification, three stages log-detection for magnitude estimation, conversion of the 125 KHz signal to audio band (1 KHz – for further digital signal processing (DSP) on a computer or a special real-time DSP board) and analog demodulation. An inter-rock communication network was developed to improve the accuracy of relative rock location detection. With some base station measurements from controlled magnets, the inter-rock network can give accurate estimates of various rock locations. The effect of the relative orientation of two smart rocks was studied numerically.

For acoustic communication, tests were conducted in a lake with two sets of two hydrophones (receivers) deployed on two sides of the lake, respectively. An acoustic projector (transmitter) was placed in the middle of the lake. The time synchronization between multiple receivers was realized with a GPS timing module. Overall, the estimated peak indices were overestimated mainly due to significant multi-path echoes that delayed the time of arrival. It is still a challenge to estimate the time difference between two receivers that experience different frequency drifts. Strong multi-path echoes also lead to large bit detection errors, hence requiring advanced signal processing schemes such as channel estimation and equalization in combination with bit coding.

I - TECHNICAL STATUS

I.1 ACCOMPLISHMENTS BY MILESTONE

More measurements from laboratory and field tests of passive smart rocks and active smart rocks with magneto-inductive and acoustic communications were taken and analyzed in this quarter. In addition, controllable magnets were designed to create a new active smart rock for bridge scour monitoring.

Task 1.1 Optimal Passive Smart Rock – Engineering Design and Validation of DC Magnetic Passive Smart Rocks

In this quarter, the majority of the work on the passive smart rock portion has been developing characteristic data for the large-scale smart rocks as well as design and implementation of the second generation smart rock encasement design for both the passive and active smart rock monitoring systems.

Characteristic data Figs. 1-3 show results from typical field tests of the large magnets used for the passive smart rock system. Fig. 1 demonstrates a strong intensity (gradient) reading produced by the 4”×2” cylindrical magnet even at 125 ft away from the magnetometer. This verifies the usefulness of the large magnet for correlation between distance and magnetic intensity.

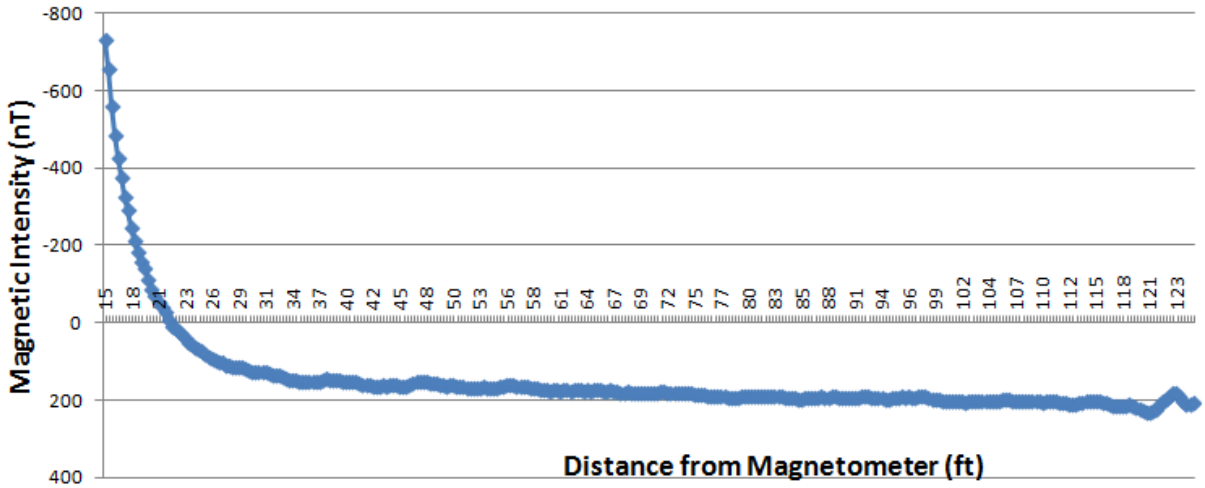

(a) Magnetic intensity vs. distance from magnetometer

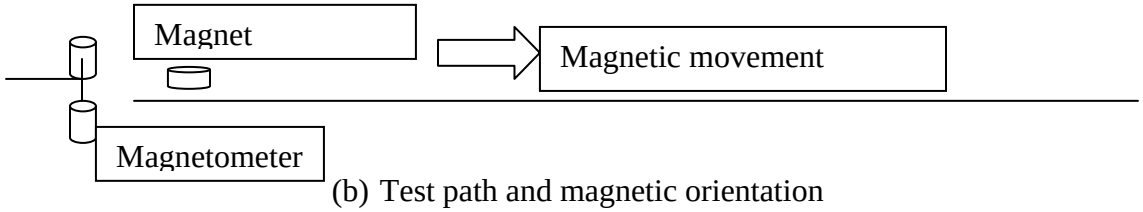

(b) Test path and magnetic orientation

Fig. 1 Characteristic Behavior of 4”×2” (diameter by thickness) Neodymium Magnet Vertically Oriented

However, Fig. 2 displays a slightly stronger intensity (gradient) as the magnet is better oriented in relation to the magnetometer. Each sensor on the magnetometer takes an independent measurement of intensity, and the gradient is the difference between the two sensors. The opposite intensity values of each pole of the magnet maximizes the gradient reading difference between the two sensors on the magnetometer.

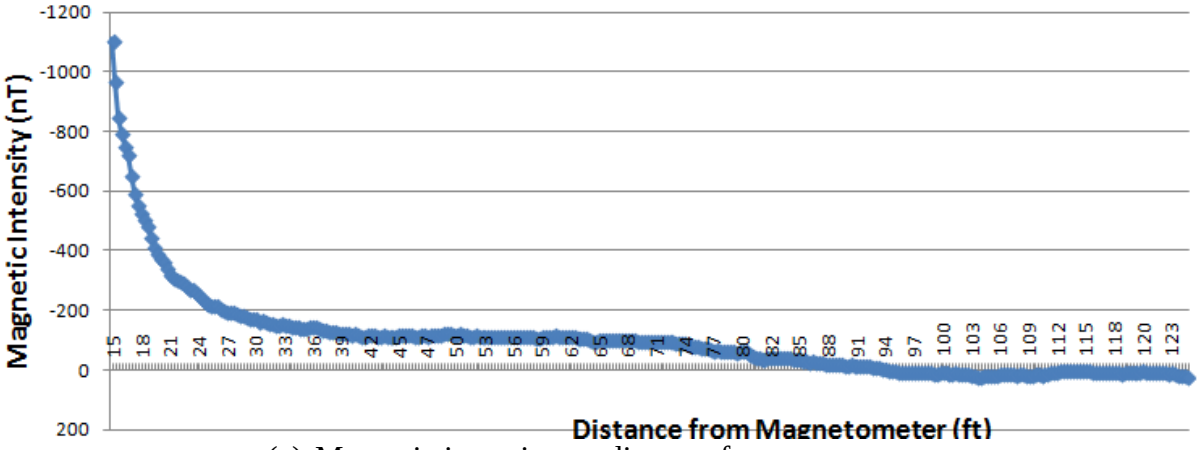

(a) Magnetic intensity vs. distance from magnetometer

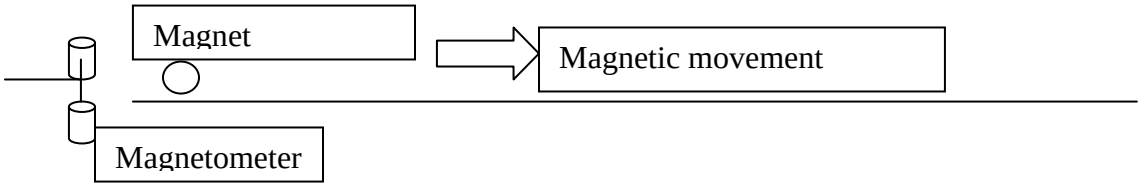

(b) Test path and magnet orientation

Fig. 2 Characteristic Behavior of 4"×2" (diameter by thickness) Neodymium Magnet Oriented Perpendicular to Test Path

Fig. 3 displays a very small change in magnetic intensity with relation to distance and a weak correlation between the two. This can be explained due to the orientation. The magnet moved parallel to the test path which was centered between the two sensors. As described earlier, the gradient is the difference between the two sensor intensity readings. Since the magnet is symmetrically located between the two sensors, the intensity change corresponding to change in distance is small. This is the worst case orientation of the magnet with relation to the magnetometer.

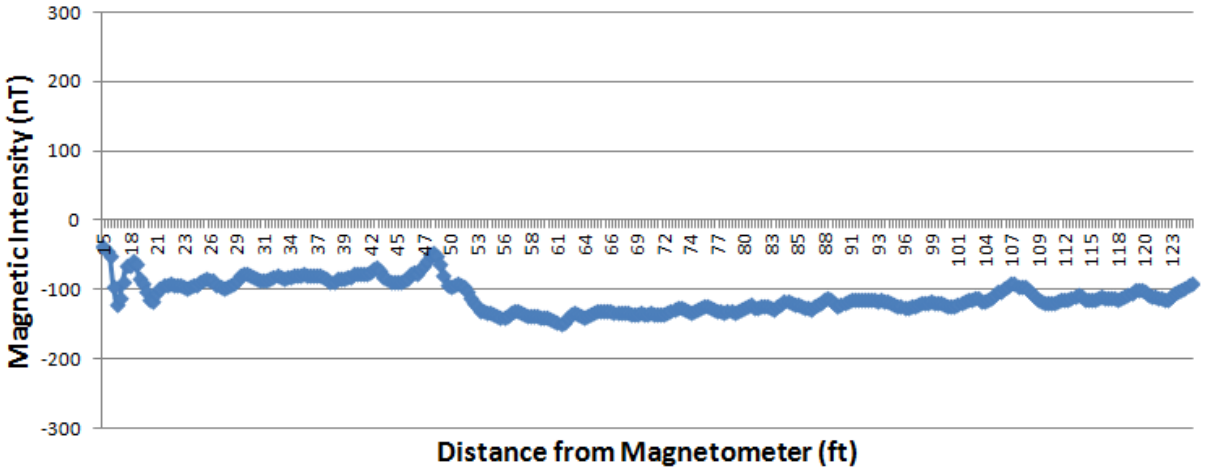

(a) Magnetic intensity vs. distance from magnetometer

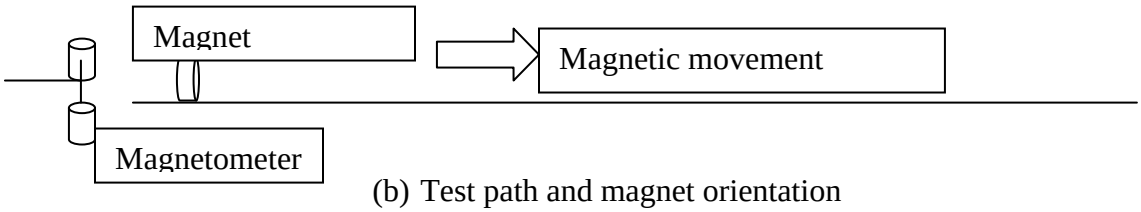

(b) Test path and magnet orientation

Fig. 3 Characteristic Behavior of 4"×2" (diameter by thickness) Neodymium Magnet Oriented Parallel to Test Path

Second Generation Passive Smart Rock The second generation passive smart rock has been finalized in this quarter of testing. It is a gravity-oriented passive smart rock. By utilizing the low friction properties inherent with a typical gyroscope apparatus, a magnet can be installed within the inner gymbol off centered to allow the magnet to consistently orient itself in the same position (gravity-oriented) no matter how the outer encasing is oriented. This, in theory, eliminates the orientation effect of the magnet on the intensity reading results. Without orientation to contend with, the distance correlation to intensity is much stronger.

Task 1.2 Steel Interferences to Magnetic Measurements – Noise Level, Data Cleansing and Engineering Interpretation with Passive Rocks Submitted

The previous report already indicated that the gradient measurement mainly removed the Earth's magnetic field. There is no clear sign of indication that the noise level in the gradient readings was reduced by the subtraction between the readings from two sensor heads of a magnetometer.

Task 2.1 Active Smart Rocks with Embedded Controllable Magnets or with Embedded Electronics – Engineering Design and Validation of Active Smart Rocks Submitted

By installing a magnet in the center of a gyroscope construction and wrapping a coil of wire around the outer gymbol, a circuit can send an electric pulse through the wire which changes the polarity and in turn flips the magnet at a constant rate. The low friction attribute of the gyroscope allows the energy consumption to be much lower than previous attempts of an active smart rock with embedded controllable magnets. The maximum and minimum amplitude of data from the

flipping smart rock can be aligned with the envelope curve of the magnetic intensity to give a more accurate distance value by eliminating the orientation effect.

Tasks 2.2(a) and 2.3(a) Magneto-Inductive Communications – Engineering Design and Validation of Magneto-Inductive Transponders Submitted

New Base Station Receiver Unit Assembly A new Base Station Receiver Unit was assembled as shown in Figs. 4 and 5. The new system can perform received Smart Rock signal filtering, amplification, three stages log-detection for magnitude estimation, conversion of the 125 KHz signal to 1 KHz audio band for further digital signal processing (DSP) on a computer or a special real-time DSP board, and analog demodulation.

Fig. 4 New Base Station Receiver Unit

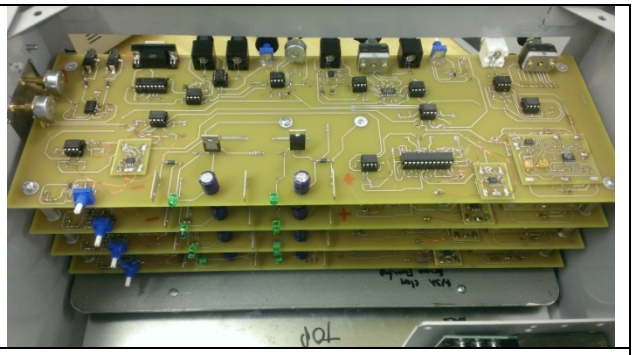

Fig. 5 New Base Station Receiver PCBs

The new assembly provides four independent channels for signal processing. The corresponding four printed circuit boards are stacked up in the enclosure with a set of connections and controls at the front panel. Each channel can be individually tuned and used as a demodulator since the COM port interface is made available at each channel (in the previously used Base Station, demodulation was only available for one of the channels, while other channels had independent filter/amplifier configurations).

RSSI Acquisition and Inter-rock Network Implementation In previous reports, communication with a smart rock unit was made possible only from a base station with a wake-up transmitter unit and a receiver. For a practical localization technique development, communication between individual rocks is now implemented, forming a network communication among smart rocks.

Received Signal Strength Intensity (RSSI) values have been acquired from rock-to-rock communication data. The RSSI dynamic range estimation in relation to the distance between rocks was performed in outdoor environment as illustrated in Fig. 6. The test setup includes main components such as transmitting smart rock antenna, receiving smart rock, and receiving base station. The transmitting smart rock electronic unit was located at the stationary place next to the base station receiver. The receiving smart rock unit was placed on a cart and moved away from the transmitter. The distance range was tested within RSSI acquisition limits. The tests were performed in three orientations between the rocks: (a). co-axial co-orientation when both rocks are perpendicular to the ground, (b). co-planar co-orientation when both rocks are parallel to the ground and located in the same plane, and (c). 90 degree cross orientation when the two rocks

(coils) are perpendicular and parallel to the ground, respectively. Fig. 7 illustrates the relative orientations of two smart rocks in three cases. The RSSI readings in dB versus distance between the rocks are presented in Fig. 8.

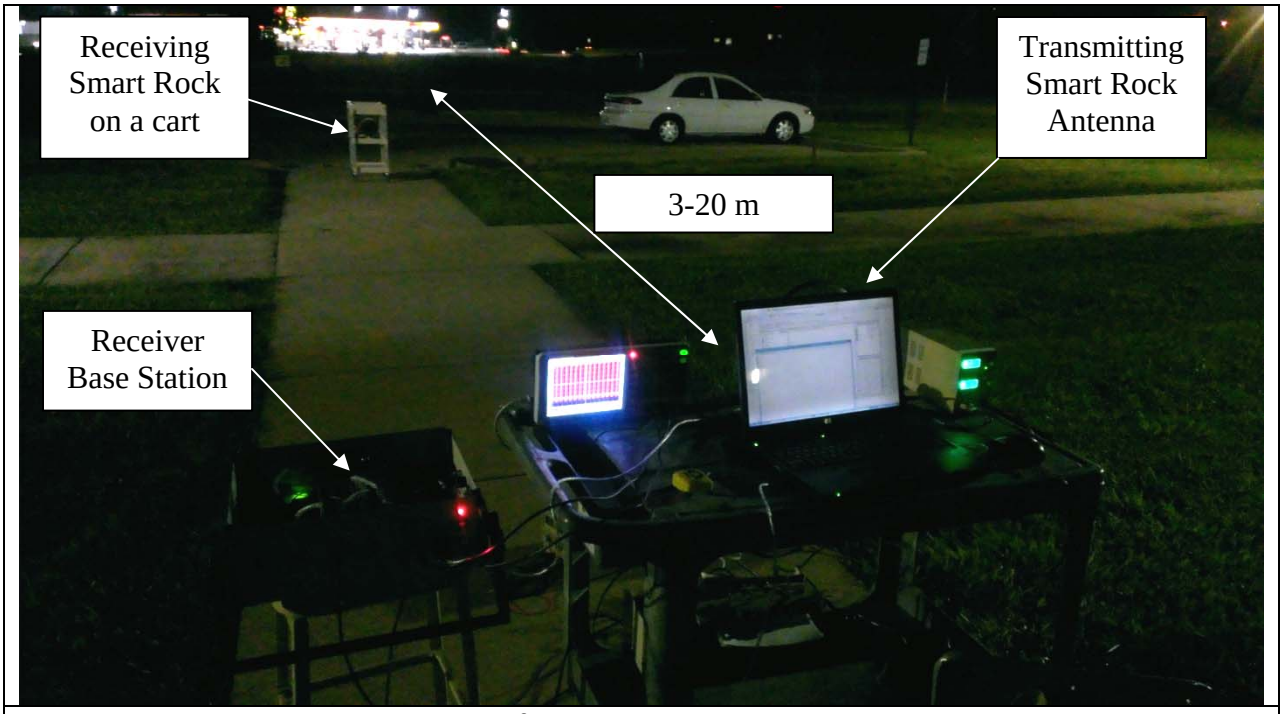

Fig. 6 Photo of the RSSI Acquisition Test Setup

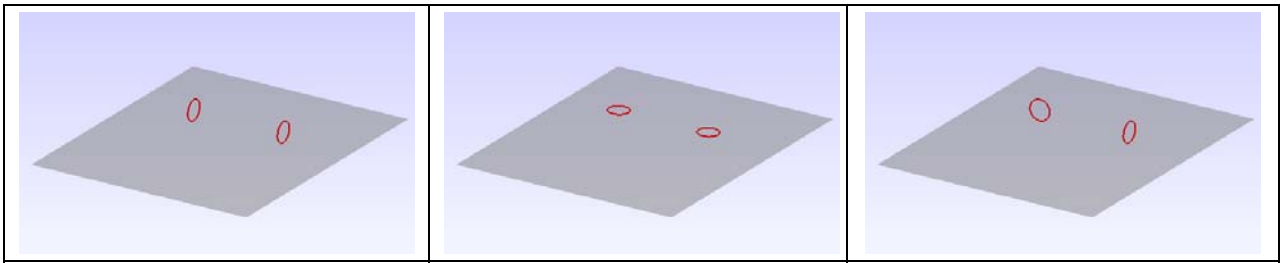

(a) Co-axial orientation | (b) Co-planar orientation | (c) 90 degree cross-orientation

Fig. 7 Relative Orientation of Two Smart Rocks (coils)

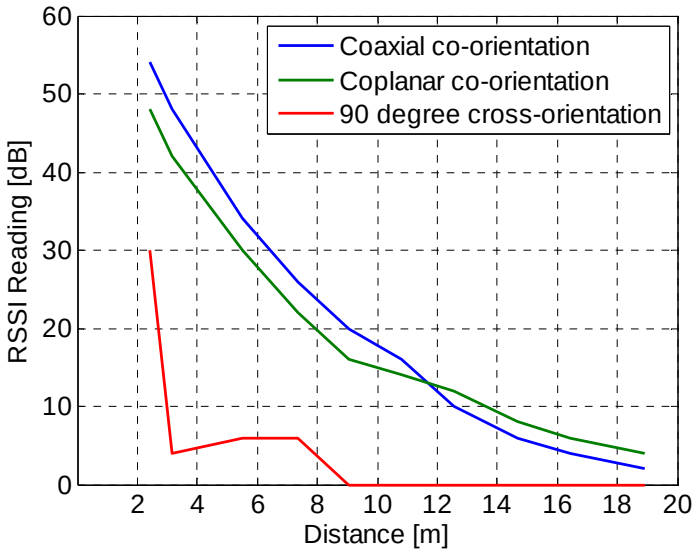

Fig. 8 Test Results on the RSSI Acquisition from an Inter-rock Network Communication

The RSSI was obtained on board using an AS3930 low frequency receiver IC, which provides ~60 dB field strength sensitivity. The performed tests demonstrated that a sensitivity of 60 dB is sufficient over 15 m measurement distance. In both co-axial and co-planar orientations, the RSSI readings were significant up to 19 m distance. Up to 11 m measurement distance, the co-planar orientation gave about 3 dB weaker RSSI reading than the co-axial orientation. As the measurement distance increases, however, the co-planar orientation had 2 dB stronger RSSI value than the co-axial orientation. This is most probably caused by the ground effect and will be further investigated. The tests in each configuration were repeated twice and RSSI estimation demonstrated excellent repeatability.

On the other hand, the RSSI estimation as shown in Fig. 8 was limited to a short range (~8 m) since loop antennas in 90 degree cross-orientation have very strong polarization loss in communication. This is a priori known issue and such an orientation between the rocks is unlikely to happen in a practical case.

The effect of antenna misalignment was analyzed in numerical modeling. Fig. 9 shows a model of a radiating impressed current source and a receiving Smart Rock antenna. The coils in the source or antenna are co-aligned. However, the receiving antenna can be positioned in various angles (0 - 90 degree) with the source. Fig. 10 shows the normalized coupled voltage as seen at the antenna port as the antenna was rotated from 0 to 90 degrees. It can be seen from Fig. 6 that the signal drops more than 30 dB with over 85 degree rotation but only 6 dB in the first 60 degree rotation.

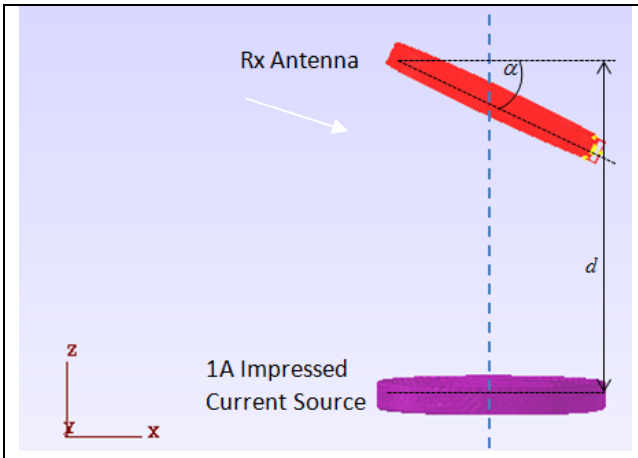

Fig. 9 Misalignment Model

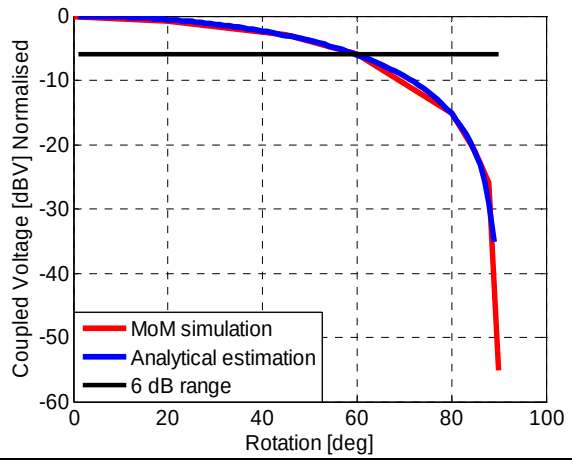

Fig. 10 Coupled Voltage vs. Alignment Angle

Localization Scheme Development A RSSI-based smart rock localization scheme is currently under development. The initial analysis was performed using full-wave modeling with the Method of Moments (EMCoS EMC Studio simulation tool). The general idea of the localization technique is to arrange communication among a set of smart rocks such that each rock sequentially pings all other rocks and gets their relative RSSI values so that, together with the base station measurements from some or all rocks, the absolute locations of all rocks can be estimated more accurately. The overall methodology is currently under development. Fig. 11 demonstrates one of the considered model configurations. Here the transmitting and receiving smart rocks are represented in purple and dark blue colors, respectively. The distances from the transmitting unit to some of the receiving units are given in Fig. 11. In this model, all of the rocks are oriented with loop-antennas being in the same plane.

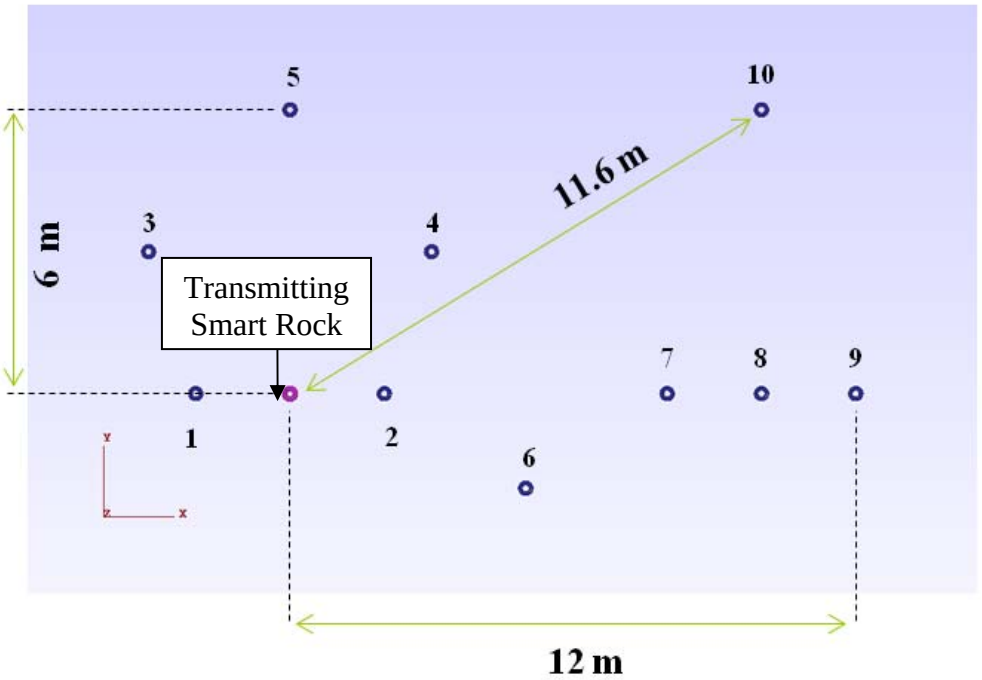

Fig. 11 A Network of 11 Smart Rock Units

Figs. 12 and 13 show the distance (from the transmitting rock to each other rock) and the RSSI data (obtained at each of the receiving rock locations), respectively. Note that the horizontal axis in Figs. 12 and 13 represents the ID of each smart rock. The vertical axis is Distance r [m] in Fig. 12 and RSSI data in Fig. 13.

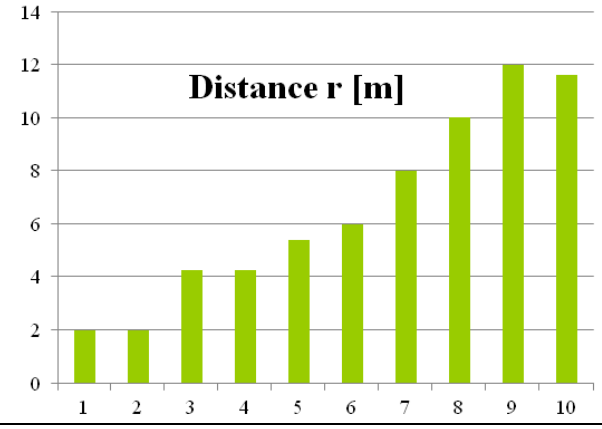

Fig. 12 Distance between Transmitting and Receiving Units

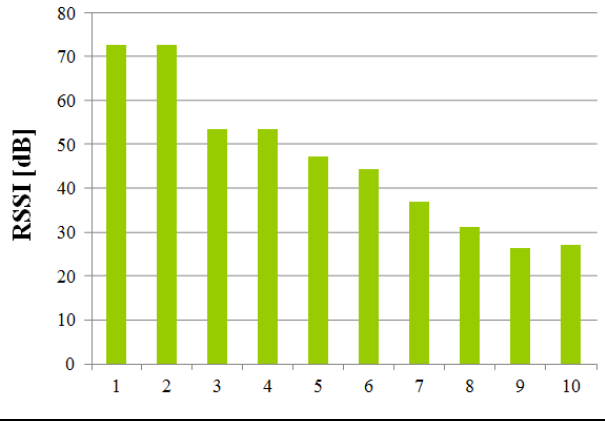

Fig. 13 RSSI Readings at Each of the Receiving Unit

The RSSI values were then related to the distances among the units by $1/r^3$. Their proportional coefficient K was identified to be 35000. However, such a simple conversion is only possible for the cases when all antennas in the network are oriented in the same way. As rocks tilt and rotate, polarization loss factor (PLF) between any two antennas increases, demonstrating strong directional characteristics. A PLF compensation scheme based on known mutual orientations of the antennas is currently under development. In practical uses, the orientation of antennas is obtained by processing readings from the accelerometer and magnetometer embedded in each smart rock unit.

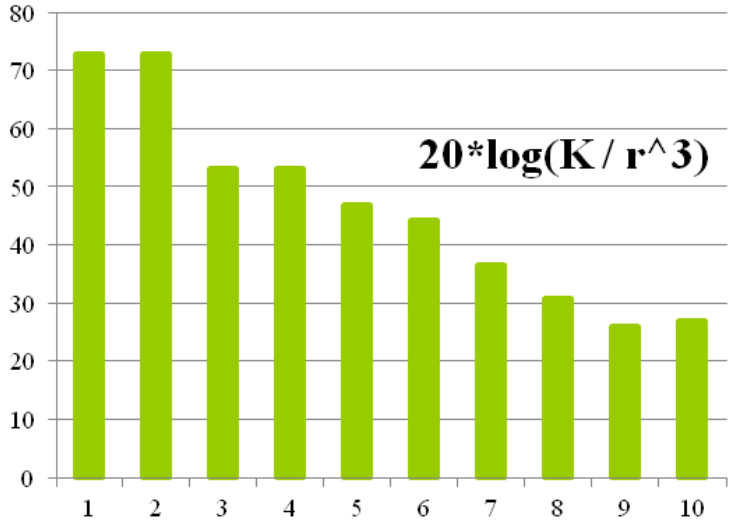

Fig. 14 Distance to RSSI Conversion

Pressure Sensor Integration An APG PT-500 submersible pressure transducer was ordered for integration into a Smart Rock unit (http://www.apgsensors.com/sites/default/files/PT-500.pdf). The photo in Fig. 15 shows a general view of the pressure sensor. The tip of the sensor contains a membrane that can be directly exposed to water. The other end of the sensor provides a watertight electrical wire for pressure acquisition. The sensor is configured for 15 psi, corresponding to 10 m water. Different configurations for up to 140 m depth are also available.

Fig.15 Photo of the APG PT-500 Pressure Sensor Unit

The pressure sensor has a simple electrical connection as shown in Fig. 16, is powered up by a voltage source of 10V-28V DC, and produces current output in the range of 4-20 mA. The Smart Rock electronic boards already contain a voltage source of 10 V, and its microcontroller has an available pin with Analog-to-Digital converter to read the sensor output. Thus, minimal design updates are required on the electronic board. However, integration of the pressure sensor into a Smart Rock unit requires specific mechanical works to ensure a watertight interface between the sensor and electronic compartment.

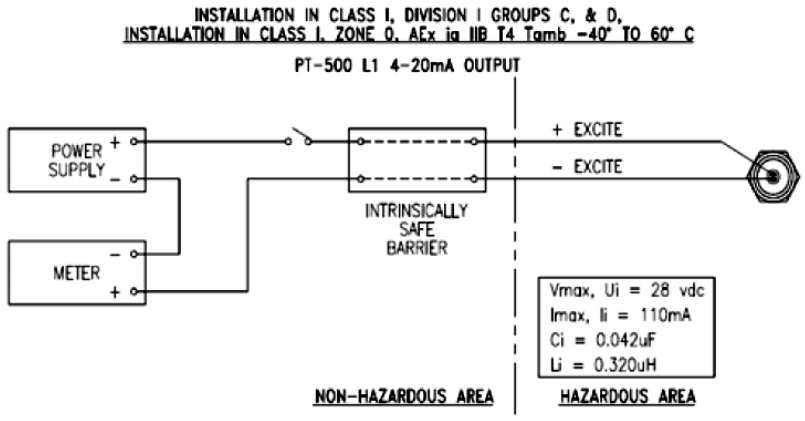

Fig.16 The Pressure Sensor Electrical Connection Scheme

Tasks 2.2(b) and 2.3(b) Acoustic Communications – Engineering Evaluation of Acoustic Communication Systems for Bridge Scour Monitoring

In this quarter, the localization method using multiple DSP receivers has been integrated and tested in three field experiments. During various tests, one transmitter (Tx) and two sets of receivers (Rx with 2 channels each) were deployed at different locations as shown in Fig. 17. When using Time Difference of Arrival (TDoA) for localization, timing synchronization among the receivers is critical to achieve satisfactory accuracy. In this study, a commercial GPS timing module has been integrated into each DSP receiver so that the data acquisitions at all receivers are synchronized with 1 pulse per second (PPS) outputs from many GPS modules. This method can mitigate the difference of sampling frequencies between the transmitter and the two receivers.

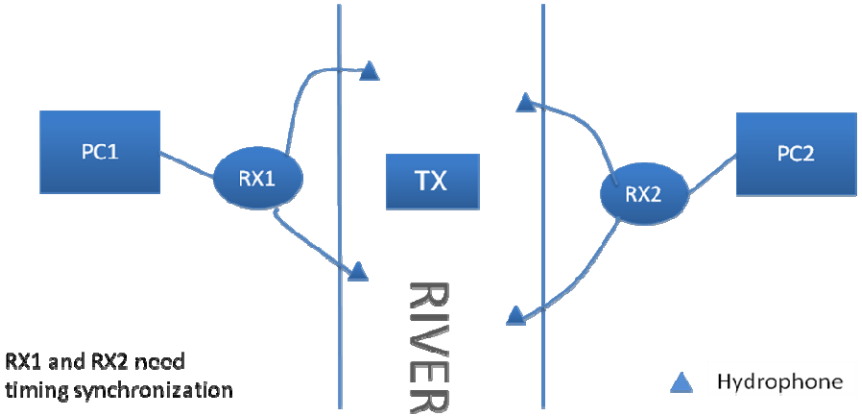

Fig. 17 Timing Synchronization Approach for Localization

The field tests were conducted at a small wooden bridge on Pine Lake near Pine Forest Drive, Rolla, MO. The bridge and its surrounding area are shown in Fig. 18. The receiver was separated from the transmitter for about 40 ft. Distinguishable signals can be received as far as 180 ft.

(a) The area of test site (b) The wooden bridge

Fig. 18 Overview of the Test Site and the Wooden Bridge near Rolla

The relative locations of the projector (transmitter) and hydrophones (receivers) are marked as #1 – #7 in Fig. 14b. Their exact locations were measured by a Total Station as presented in Table

1. Similar locations were used in the other two experiments. The transmitters at locations #5 - #7 transmitted signals one at a time in turn.

Table 1 Locations of transmitter and receivers for tests conducted on May 29, 2013

Points	(x, y) coordinates (ft)	Tx/Rx	Transducer type
1	(-42.829, 36.725)	Rx1 ch1	BII Hydrophone
2	(-56.475, -32.045)	Rx1 ch2	BII Hydrophone
3	(-6.596, 40.353)	Rx2 ch1	BTech Transducer
4	(-12.120, -44.261)	Rx2 ch2	BTech Transducer
5	(-26.755, 11.860)	Tx	BTech Transducer
6	(-22.687,7.408)	Tx	BTech Transducer
7	(-27.569, 8.090)	Tx	BTech Transducer

Very strong interference was also observed during the first two field tests and it resulted from the regular power invertors (Power Bright PW2300-12 2300) that were used to supply 110 V AC power to the receivers. To remove the signal interference, high quality power invertors (Power Bright APS-300-12) were used. Even so, the signals received at all channels were still very noisy and contained very long and strong multi-paths as indicated in Fig. 19. The multi-path delay spread was as large as 40 – 50 bits long in Receiver 1 as can be seen in Fig. 19 that the large signal smeared into the gap between the last bit of the current block and the first bit of the next block. The results are severe inter-symbol interference and large errors in bit detection and TDoA estimation. The echo path in Receiver 2 was smaller at about 10 bits long and the SNR was a few dB higher than Receiver 1.

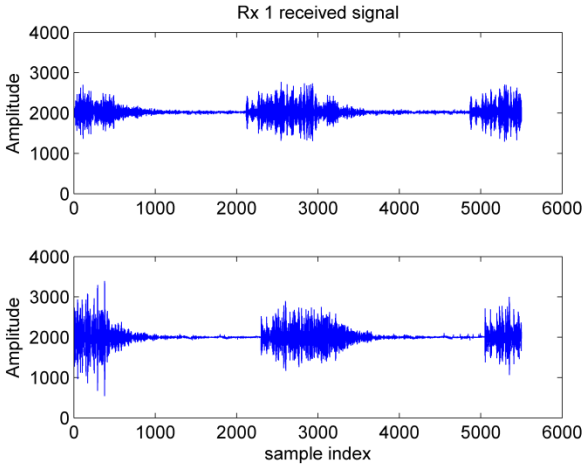

(a) Receiver 1: strong signals with significant echoes and noise

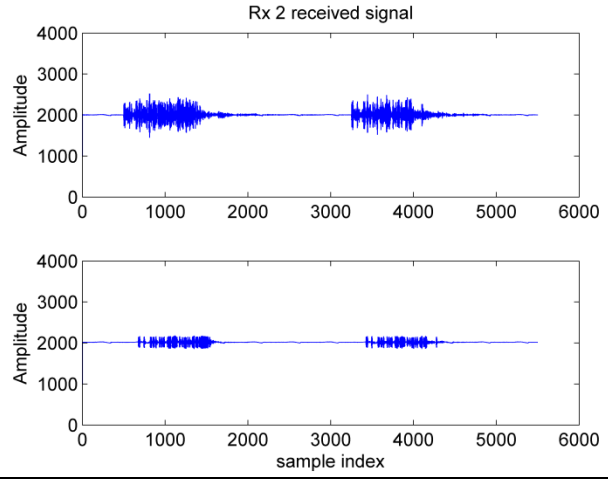

(b) Receiver 2: weak signals with good SNR and low echoes

Fig. 19 Received Signals from Four Channels on May 29, 2013

The TDoA was estimated by first correlating the received pass band signals with the up-sampled 63-bit PN sequence and then detecting the correlation peak. The sample index corresponding to the peak is considered to be the first arrival of the PN sequence as indicated in Fig. 20. The index was used to compute the TDoA for transmitter localization. During tests, three challenges were encountered:

1. Two peaks may be present in each acquisition of the two channels per receiver, e.g. in Fig. 20b.
2. Multi-path echoes may cause large estimation errors in the detected peak index as shown in Fig. 21. The peaks mostly arrived at a late time due to multiple reflections (non-line of site).
3. Sampling frequencies between transmitter and receivers may drift and thus cause estimation errors as illustrated in Fig. 22. Specifically, the sampling frequency drift in Receiver2 (CH3&4) was very large and changed over time. The drift in Receiver1 (CH1&2) was small with significant estimation errors due to low SNR, especially in CH1.

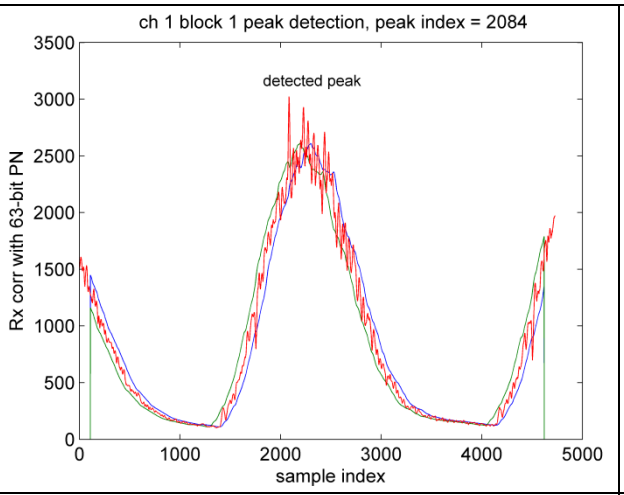

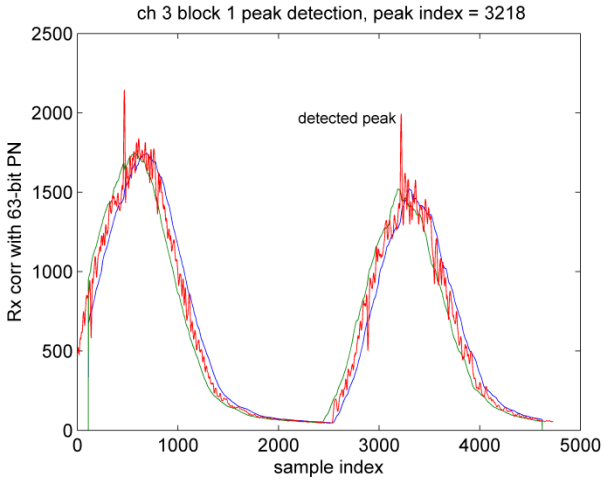

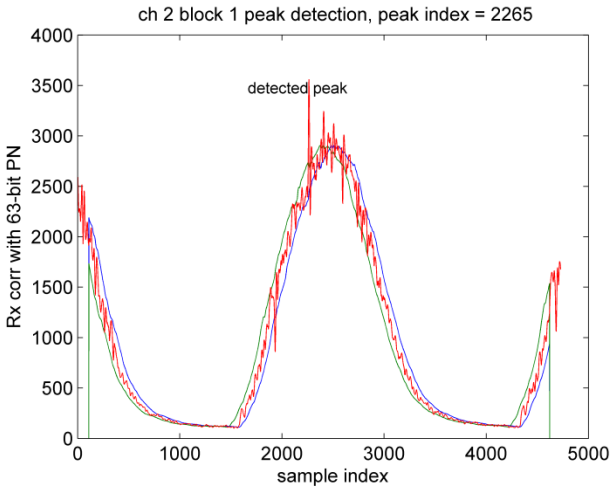

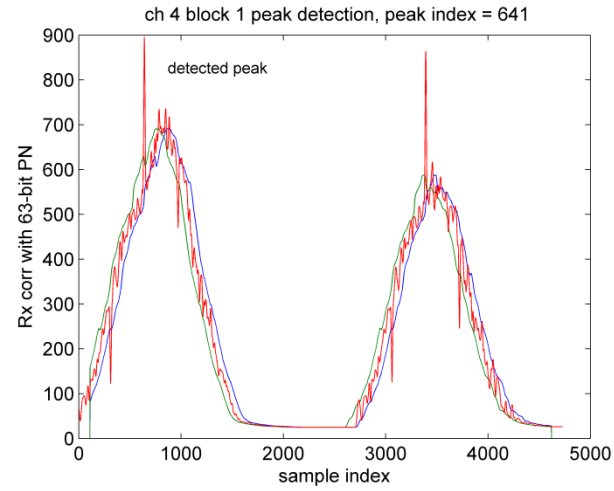

a) Peak detected from Rx1: Ch1 index = 2084 and Ch2 index = 2265

b) Peak detected from Rx2: Ch3 index = 3218 (2nd peak) and Ch4 index = 641 (1st peak)

Fig. 20 Detection of First Arrival Using 5500 Samples per Second

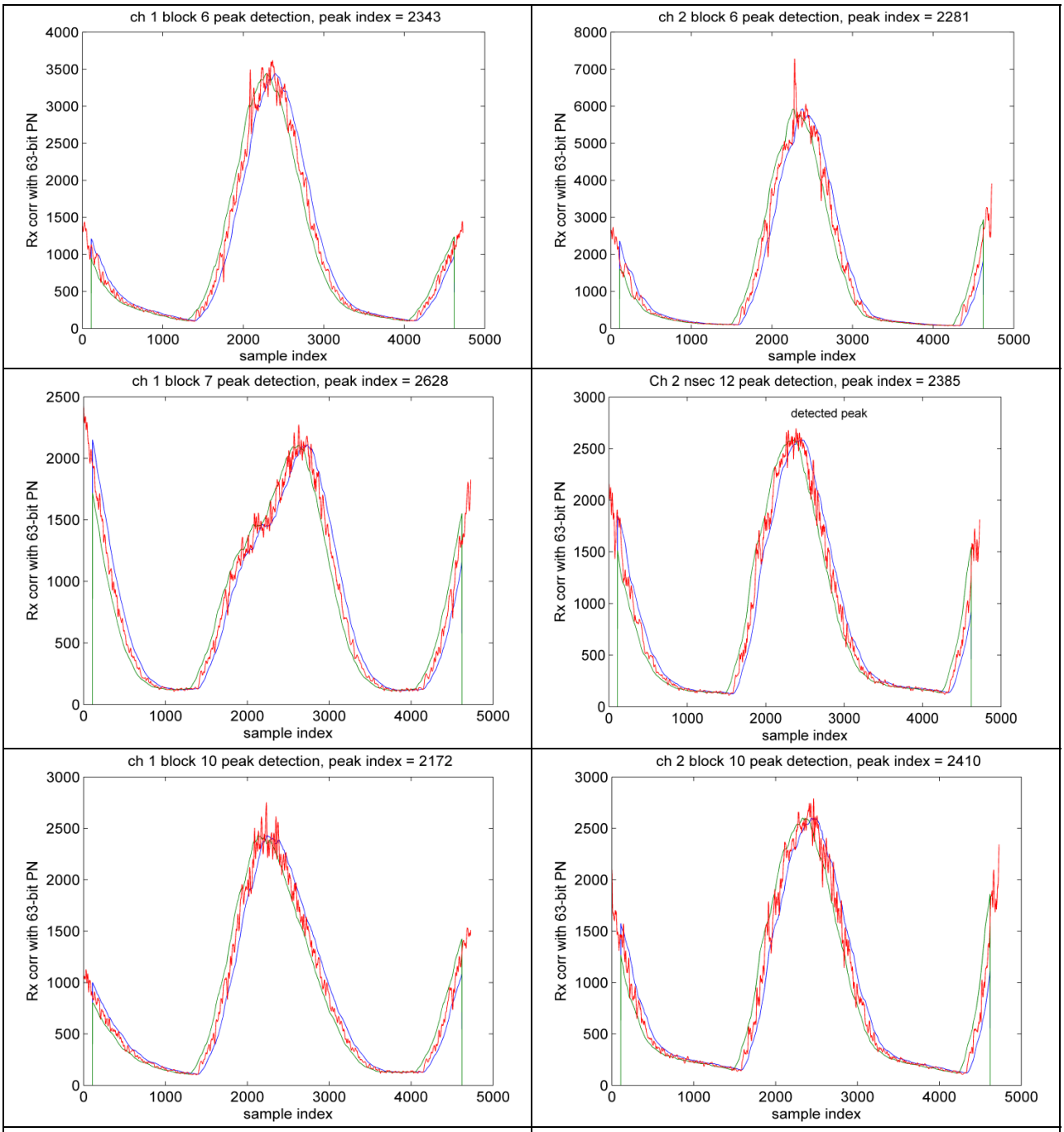

a) Rx1 Ch1: true peak index = 2085

b) Rx1 Ch2: true peak index = 2268

Fig. 21 False Detection of TDoA in Receiver1

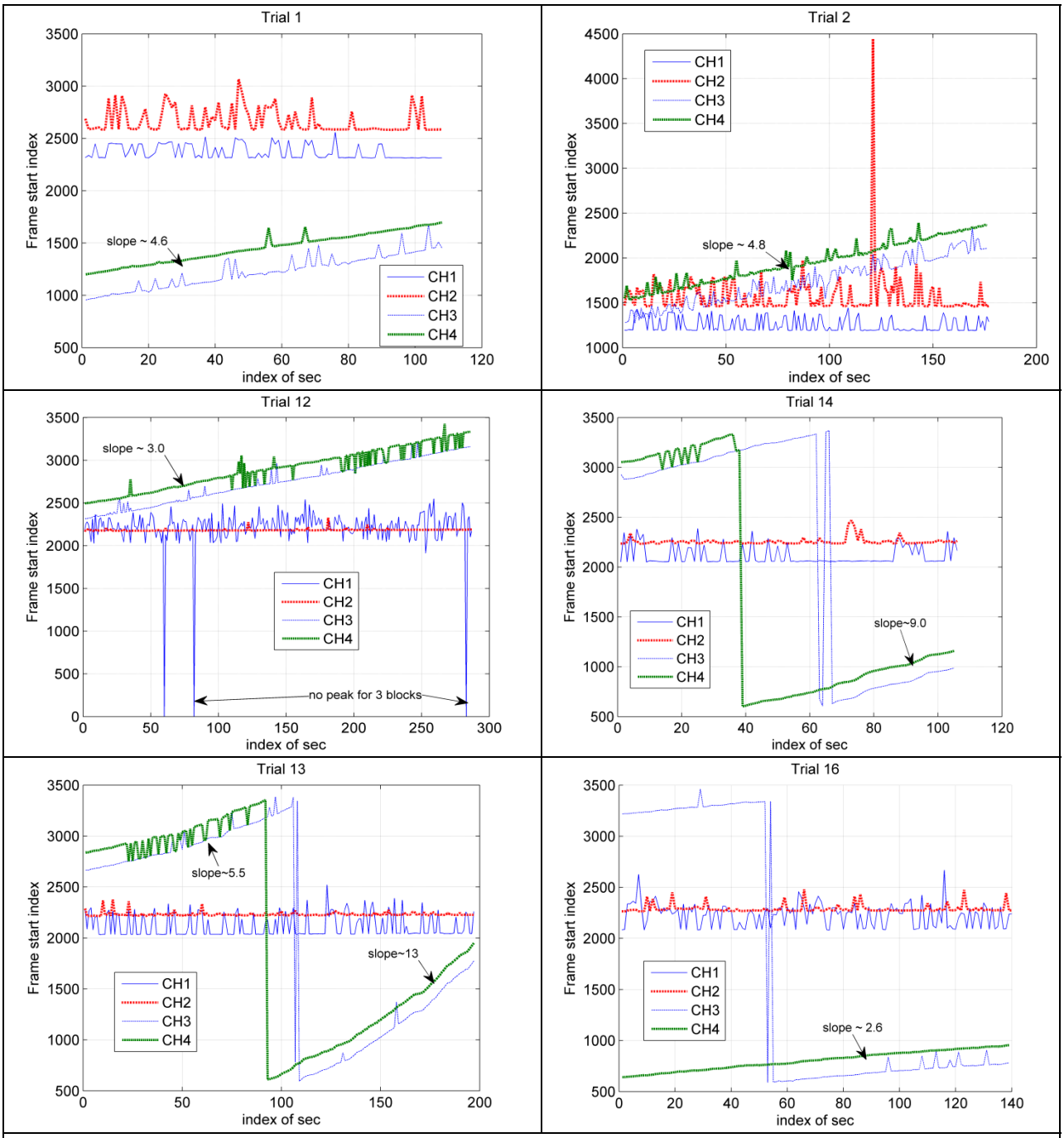

Fig. 22 Peak Detection of All Four Channels

Some observations can be made from Figs. 20-22. First, the estimated peak indices in Receiver1 are larger than the true indices mainly due to the strong multipath echoes that delayed the time of arrival. Second, the slopes of indices in Receiver2 (CH3&4) are due to frequency drift. The TDoA between the two channels with similar drifts only can be estimated accurately. Third, when there is a large error in peak detection, the bit detection experiences a large BER (Bit-Error-Rate). Good BER performance also corresponds to good peak detection. However, accurate peak detection may not guarantee good BER performance.

Remedies to the problems encountered in the field experiments are proposed here:

1. Replace the BII hydrophones used in Receiver1 by BTech transducers. BTech transducers have better quality (bandwidth and sensitivity) than BII ones, and it will significantly improve the SNR of signals.
2. Refine the low-noise amplifiers to improve the SNR of received signals. It is also desirable to add Automatic Gain Control (AGC).
3. Increase the PN sequence length and add bit encoding for payload. These can improve the robustness against multi-path echoes and improve the decoding performance. Implement equalization schemes to mitigate the inter-symbol interference.
4. Use index in the transmitted payload to identify the block numbers. This can help identify which peak was detected if two peaks are present in the acquired data window and the TDoA estimation can be corrected accordingly. This also helps to correct various frequency drifts in multiple receivers.
5. If feasible, modify the synchronization technique to include atom clocks in all transmitters and receivers so that frequencies of all parties are synchronized.
6. Refine the TDoA estimation algorithm to remove outliers: the blocks with a large Bit-Error-Rate (BER) can be simply discarded. Statistical decision methods can also be used to improve estimation accuracy.

Task 3.1 Data Fusion from Passive and Active Rocks – Scour Depth

The field tests with the second-generation smart rocks will be conducted on July 23 and 25. The distance data sets from both passive and active smart rocks will be fused together to more accurately extract mission-critical depth information for scour monitoring.

Task 3.2 Field Validation Planning and Execution – Field Test Plan and Data Analysis Submitted

Field monitoring and tests with the second-generation smart rocks are set for July 23 and 25, 2013. The results will be reported towards the end of this project.

I.2 PROBLEMS ENCOUNTERED

There are no problems encountered in this quarter. However, the project continued to be delayed for about three months as explained in the previous reports. On the other hand, the project expenditure is in general agreement with the project progress.

I.3 FUTURE PLANS

The following subtasks will be executed during the next quarter.

Task 1.1 Design, fabricate, and test in laboratory and field conditions DC magnetic sensors with embedded magnets aligned with the earth gravity field. Summarize and document the test results and the performance of passive smart sensors.

The field test data collected at bridge sites in late summer, 2012, will be further analyzed to demonstrate the effectiveness of a simple localization scheme following the triangulation strategy. In addition, the second-generation passive smart rock with a gravity-oriented magnet will be tested and characterized in upcoming laboratory and field tests.

Task 2.1 Design, fabricate, and test in laboratory and field conditions active smart rocks with embedded controllable magnets or with embedded electronics. Summarize and document the test results and the performance of active smart rocks.

Further development activities include:
- Optimization of the magnet flipping circuitry
- Gyroscope data processing for movement trajectory recovery tests

Tasks 2.2(a) and 2.3(a) Design, fabricate, and test in laboratory and field conditions magneto-inductive transponders. Summarize and document the test results and the performance of transponders.

Further development activities include:
- New field tests with Smart Rock v3 at bridges
- Inter-rock communication extensions
- Pressure sensor integration into a Smart Rock unit concrete shell
- Development of localization schemes using inter-rock RSSI data with polarization loss factor compensation
- Implementation of commands protocol to Smart Rock sensors remote reconfiguration

Tasks 2.2(b) and 2.3(b) Research, summarize, and document current underwater acoustic transmission practices and required modifications for bridge scour monitoring.

Future works for the next three months include:
- Refine localization algorithms with distributed receivers using TDoA estimates,
- Improve the BER performance by developing low-complexity equalization algorithm and bit detection algorithms, and
- Further test the localization algorithm in field experiments and improve the robustness against environmental changes.

Task 3.1 Fuse the measured data from passive and active smart rocks to extract mission-critical data for scour monitoring

The field test data from passive and active smart rocks, obtained from the upcoming July 2013 tests, will be fused to better estimate the maximum scour depth for bridge scour monitoring.

Task 3.2 Plan and execute the field validation tasks of various prototypes. Analyze the field performance of smart rocks and communication systems.

Field tests at two bridge sites were scheduled to take place on July 23 and 25, 2013. The field test data will be processed to evaluate the field performance of various technologies.

II – BUSINESS STATUS

II.1 HOURS/EFFORT EXPENDED

The planned hours and the actual hours spent on this project are given and compared in Table 2. In the eighth quarter, the actual hours are less than the planned hours, leading to an actual cumulative hour of approximately 68% of the planned hours. The cumulative hours spent on various tasks by personnel are presented in Fig. 23.

Table 2 Hours spent on this project

	Planned		Actual	
	Labor Hours	Cumulative	Labor Hours	Cumulative
Quarter 1	752	752	163	163
Quarter 2	752	1504	436	599
Quarter 3	752	2256	381	979
Quarter 4	752	3009	177	1157
Quarter 5	720	3729	721	1877
Quarter 6	720	4449	1069	2946
Quarter 7	720	5169	769	3715
Quarter 8	720	5889	285	3999

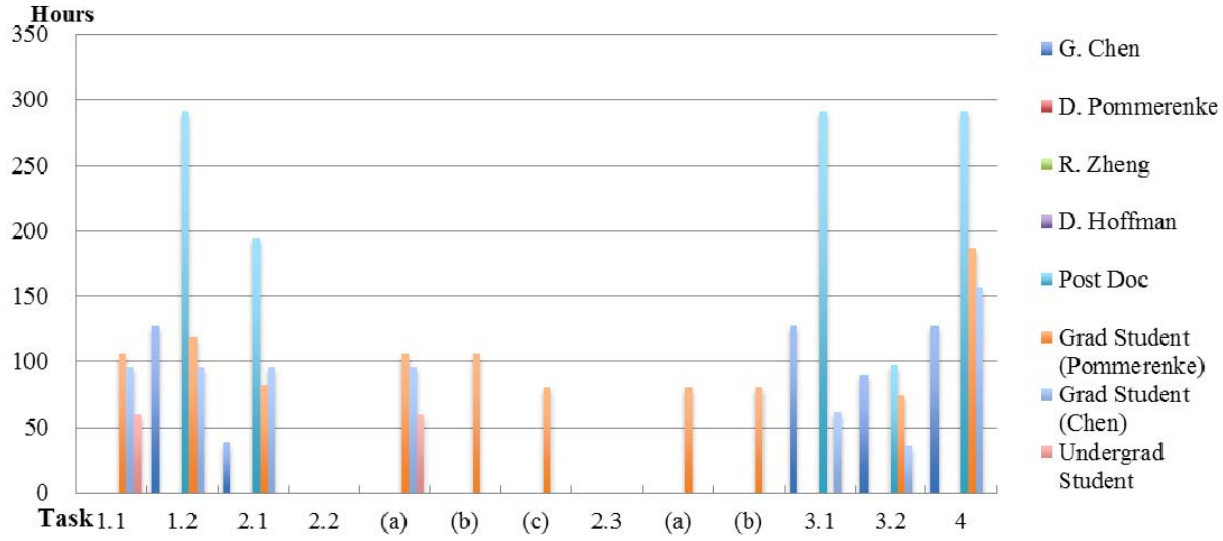

Fig. 23 Cummulative Hours Spent on Various Tasks by Personnel

II.2 FUNDS EXPENDED AND COST SHARE

The budgeted and expended RITA funds accumulated by quarter are compared in Fig. 24. Approximately 77% of the budget has been spent till the end of eighth quarter. The actual cumulative expenditures from RITA and Missouri S&T/MoDOT are compared in Fig. 25. The expenditure from RITA is less than the combined amount from the Missouri S&T and MoDOT.

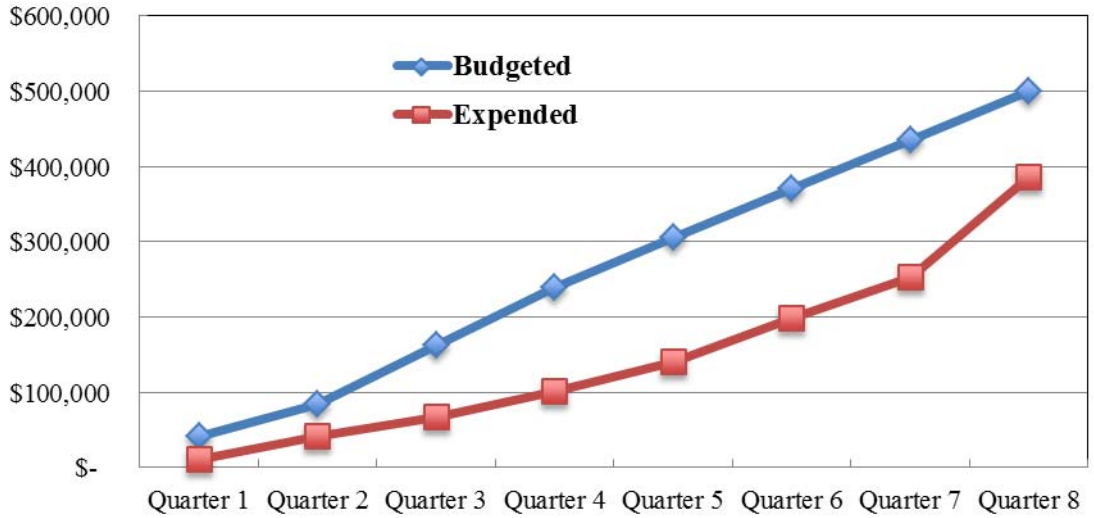

Fig. 24 Comparison of RITA Budget and Expenditure Accumulated by Quarter

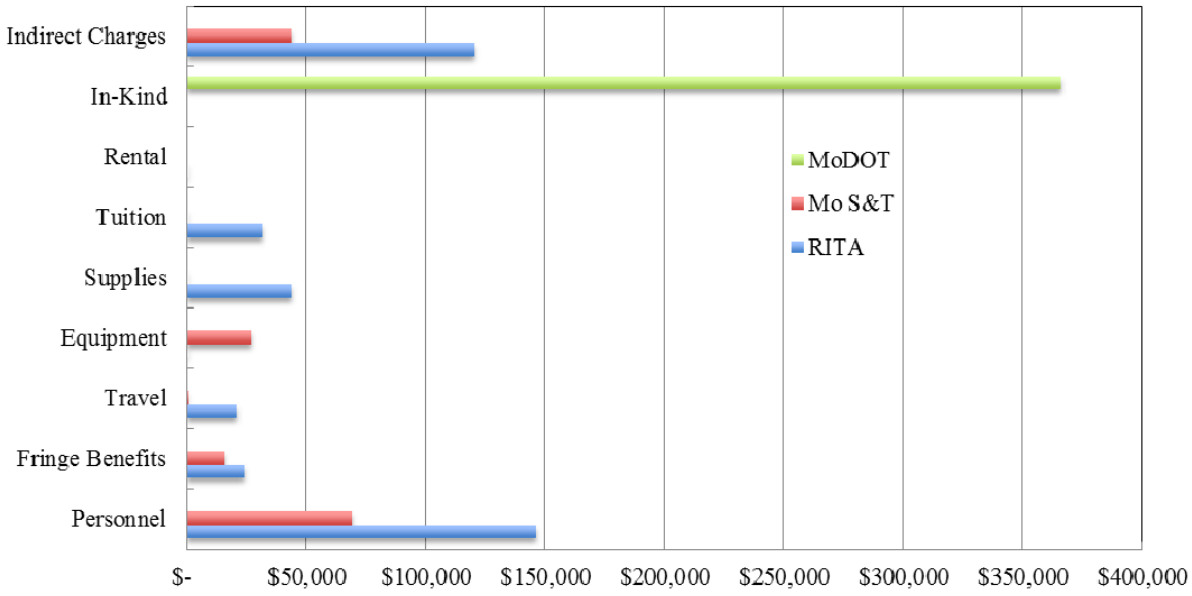

Fig. 25 Cummulative Expenditures by Sponsor